Acta Med. Okayama, 2012
Vol. 66, No. 5, pp. 409–415

Acta Medica Okayama
http://escholarship.lib.okayama-u.ac.jp/amo/

Original Article

Dynamic Finite Element Analysis of Impulsive Stress Waves Propagating from Distal End of Femur

Takaaki Sarai[a]*, Takayuki Inoue[b], Kazuo Fujiwara[c], and Koichi Kuramoto[b]

[a]Division of Industrial Innovation Sciences, Graduate School of Natural Science and Technology, Okayama University, Okayama 700–8530, Japan, [b]Nakashima Medical Co., Ltd., Okayama 709–0625, Japan, and [c]Department of Orthopaedic Surgery, Okayama University Hospital, Okayama 700–8558, Japan

The human femur is subjected to an impulsive load at its distal end during daily life. Femoral bone fracture caused by impact loading is common in elderly women. It is important to clarify the dynamic response of the femur and to evaluate the change in its stress state during impact loading. A 3-dimensional model of the femur was prepared in the present study, and the impulsive stress waves propagating from the distal end of the femur were analyzed by the dynamic finite element method. This model showed that the von Mises equivalent stress is large on the anterior and posterior sides of the mid-diaphysis when the impact direction is different from that of the bone axis. As for the femoral neck, the absolute value of minimum principal stress initially increases on the medial side; slightly later the maximum principal stress increases on the lateral side. In this case, the absolute value of the maximum principal stress was found to be larger than that of the minimum principal stress, and the absolute value of the principal stress decreased as the impact angle increased. Further, the femoral neck and the trochanter were shown to have a higher risk of bone fracture when the impact direction is coincident with the bone axis.

Key words: biomechanics, femur, impulsive stress wave, impact angle, dynamic finite element analysis

Finite element analysis has long been used to examine human hip joints and femurs, and the risk of femoral bone fracture has been studied using a biomechanical approach [1–9]. Although there are clinical cases of elderly people breaking a femur in response to the impulsive load, the research has mainly focused on the effects of static loads such as a one-legged stance. The femur is subjected to an impulsive load at its distal end during walking or when going up and down the stairs. It is important to study the femur's response to such dynamic loads, especially in people suffering from osteoporosis [10–12]. Of course, it is difficult to evaluate impulsive stress on the femur experimentally *in vivo*.

We thus constructed a 3-dimensional model of the femur using CT images and analyzed the dynamic stress on the femur by employing the explicit finite element method. We focused on the impulsive stress wave propagating from the distal end of the femur and analyzed the stress state in the diaphysis and the stress concentration in the femoral neck. The impulsive load was applied for different directions at the distal end of the femur, and we examined the influence of the impact direction on the stress wave. The purpose of this study was to evaluate the types of dynamic stress that could lead to bone fracture and to determine where this stress wave propagates in the femur.

Received January 10, 2012; accepted May 7, 2012.
*Corresponding author. Phone:+81–86–251–8030; Fax:+81–86–251–8266
E-mail:sarai@mech.okayama-u.ac.jp (T. Sarai)

Materials and Methods

The finite element model was constructed from CT images of the right femur of an adult man. The contour lines of the cortical bone and the cancellous bone of the femur were extracted from CT images with slices at a 5-mm pitch. The software Mimics 10 (Materialise) was used for the extraction of the contour lines, and the results were output in IGES format. The solid model was created from the IGES data divided into 4-node tetrahedral elements using the software NX I-deas 5 (UGS). The generated finite element mesh consisted of 3,305 nodes and 13,780 elements for the model. The cortical and cancellous bones were modeled, and the length of the femur was modeled at approximately 414 mm.

The bone was assumed to be isotropic in the elastic deformation. The elastic moduli of the cortical bone and the cancellous bone were 7 GPa and 1 GPa, respectively, and Poisson's ratio was 0.3 for both types of bone. The density of the bones was needed for a dynamic analysis, and densities of 1,700 kg/m^3 and 1,100 kg/m^3 were used for the cortical bone and the cancellous bone, respectively. These values of material constants were determined by referring to the data book [13]; physiological parameters, *e.g.*, of different-age subjects, were not considered in this study.

As shown in Fig. 1, a rigid wall was set horizontally at the distal end of the femur and impact was applied in the vertical direction by hitting the femur against the wall. In this case, the approaching speed of the femur was 1 m/sec for every impact angle. The impact angle θ was defined as the angle between the impact direction and the bone axis in the sagittal plane, and the angles used in the analysis were 0, 30, 60, and 90 degrees. These impact angles were set considering the height of a stair step, for example. The rigid wall was attached to several element surfaces including the lowest node of the model for each impact angle. The displacements of the nodes facing the wall were restricted for the stable impact; namely, the displacements were fixed in the plane perpendicular to the impact direction.

The program used for the calculation was MSC. Marc 2008 (MSC. Software), and the changes of the stress state were evaluated using the dynamic explicit method in finite element analysis. The calculation was repeated until the elapsed time $t = 450\,\mu$sec after the start of hitting the femur against the wall at time intervals of $\Delta t = 5 \times 10^{-8}$sec.

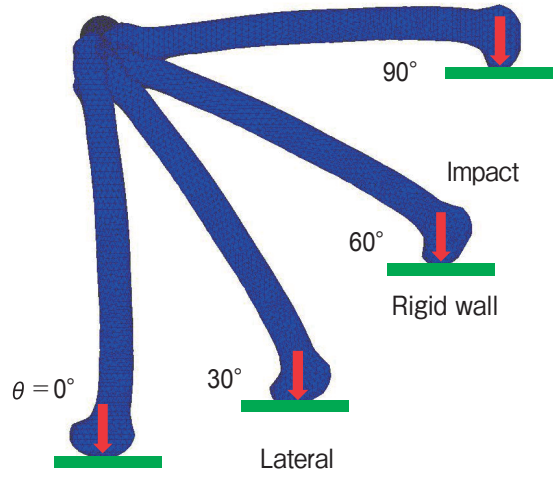

Fig. 1 Boundary condition of dynamic finite element analysis. Impact is applied by hitting the distal end of the femur against a rigid wall with an approaching speed of 1 m/sec. The angle between the impact direction and the bone axis in the sagittal plane is defined as the impact angle θ.

Results

The stress distributions of the cortical bone surface in the anterior view of the model are represented in Fig. 2. The von Mises equivalent stress was employed here, and the results of the impact angle $\theta = 0$, 60 degrees at $t = 100$, 200, 300, 400 μsec are shown in the figure. The propagation of the stress wave was confirmed, and the wave reached the femoral neck at $t = 300\,\mu$sec. The stress distribution in the case of $\theta = 0°$ was different from that of $\theta = 60°$, indicating that the propagation of the stress wave was dependent on the impact angle. The stress states of the femoral mid-diaphysis and the proximal femur with the impact angle of $\theta = 0°$ were compared with those of $\theta = 60°$ in the following results.

The distributions of the equivalent stress in the femoral mid-diaphysis at $t = 200$, 300 μsec are shown in Fig. 3, where the distributions were those in the cross section perpendicular to the bone axis. The stress of the cortical bone was large compared with that of the internal cancellous bone in the case of $\theta = 0°$, and the stress was distributed uniformly in each

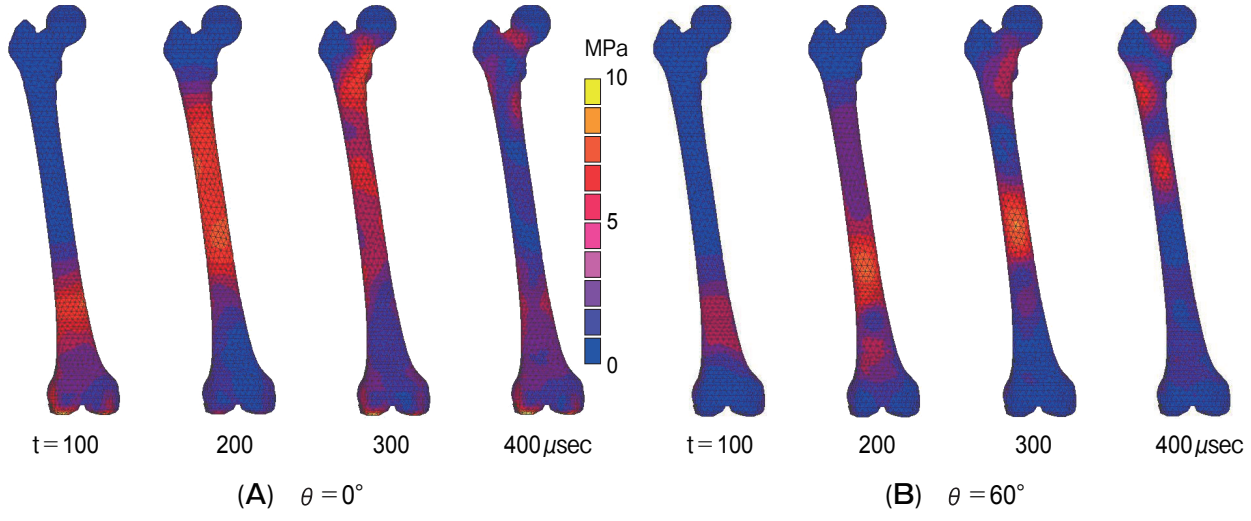

Fig. 2 Propagation of the stress wave in the cortical bone surface of the femur in the case of $\theta = 0°$ (**A**), 60° (**B**). Distributions of equivalent stress at t = 100, 200, 300, 400 μsec are shown.

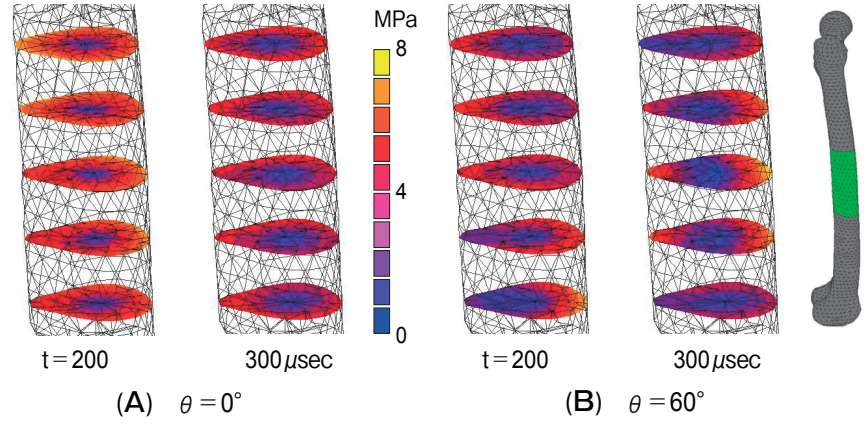

Fig. 3 Distribution of equivalent stress in the femoral mid-diaphysis in the case of $\theta = 0°$ (**A**), 60° (**B**). Stress distributions are represented in a cross section perpendicular to the bone axis at t = 200, 300 μsec. The green area shows the mid-diaphysis in the femur used to represent the stress distribution.

bone. Meanwhile, the stress distribution depended on the selected cross section and the elapsed time in the case of $\theta = 60°$. A large equivalent stress was found distinctively on the anterior and posterior sides at t = 300 μsec.

The stress of the diaphysis fluctuated with the elapsed time during the impact loading. The change of the stress in the cortical bone surface is shown in Fig. 4(A). Namely, the time histories of the equivalent stress of the nodes located on the anterior, posterior, medial, and lateral sides of the mid-diaphysis were evaluated. The nodes used were located around the cross section of the mid-diaphysis shown in the figure. The stress on the anterior side at around t = 330 μsec was very large, except for at $\theta = 0°$, and the stress on the posterior side also became large for $\theta = 60°$ and 90°. Fig. 4(B) represents the similar time histories of the maximum and minimum principal stress for the same 4 nodes used in Fig. 4(A). The difference in the stress on the 4 sides was relatively small in the history of $\theta = 0°$. However, the difference in the absolute values between the maximum principal stress on the posterior side and the minimum principal stress on the anterior side at around t = 330 μsec became

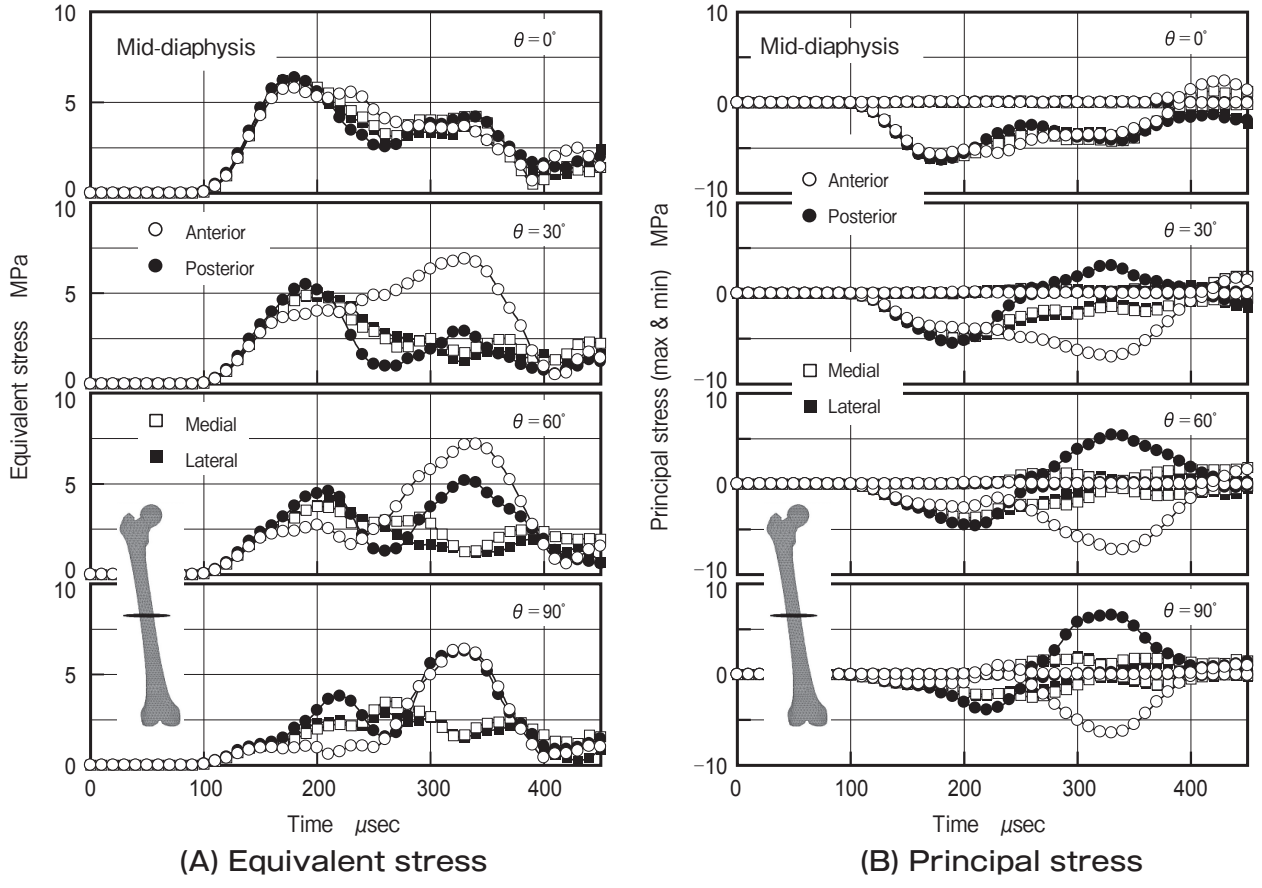

Fig. 4 Time history of stress in the cortical bone surface of the mid-diaphysis. Changes of equivalent stress (A) and principal stress (B) with elapsed time are evaluated for 4 nodes located around the cross section of the mid-diaphysis shown in the figure.

remarkable as the impact angle increased.

The distributions of the equivalent stress in the proximal femur at $t = 280,\ 380\,\mu$sec are shown in Fig. 5. The stress wave reached the medial side of the femoral neck at $t = 280\,\mu$sec and reached the lateral side at $t = 380\,\mu$sec. A large stress was found in the cortical bone surface, as is shown by the distribution in the cross section. The stress in the results of $\theta = 0°$ was larger than that of $\theta = 60°$. The stress of the femoral head and the greater trochanter was small compared with that of the femoral neck and the lesser trochanter.

The stress concentration was found in the femoral neck, as mentioned above, so we examined the time history of the equivalent stress in the cortical bone surface around the femoral neck. Fig. 6(A) shows the changes of the stress on the anterior, posterior, medial, and lateral sides of the neck. The stress became large at around $t = 270\,\mu$sec, except for the lateral side in the case of $\theta = 0°$. The stress on the lateral side increased again after $t = 270\,\mu$sec, and the stress at $t = 380\,\mu$sec was the largest of the 4 sides. As the impact angle increased, the change in the level of stress became small on every side of the femoral neck. Corresponding to Fig. 6(A), Fig. 6(B) represents the changes in the maximum and minimum principal stress. As shown in the results of $\theta = 0°$, the minimum principal stress was compression on the anterior and medial sides, and the absolute value of the minimum principal stress was larger than that of the maximum principal stress. The compressive principal stress changed into tensile stress during the propagation of the stress wave on the posterior side. The maximum principal stress on the lateral side was always tensile, and was the largest tensile stress in all reference nodes, including the mid-diaphysis shown in Fig. 4(B).

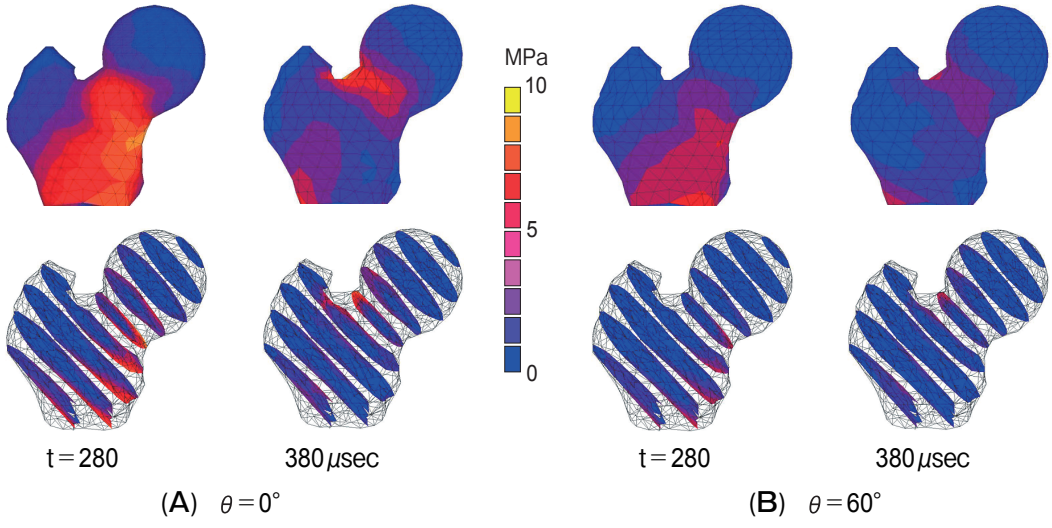

Fig. 5 Distribution of equivalent stress in the proximal femur in the case of $\theta = 0°$ (A), 60° (B). Stress distributions in the cortical bone surface and those in the cross section at t = 280, 380 μsec are shown.

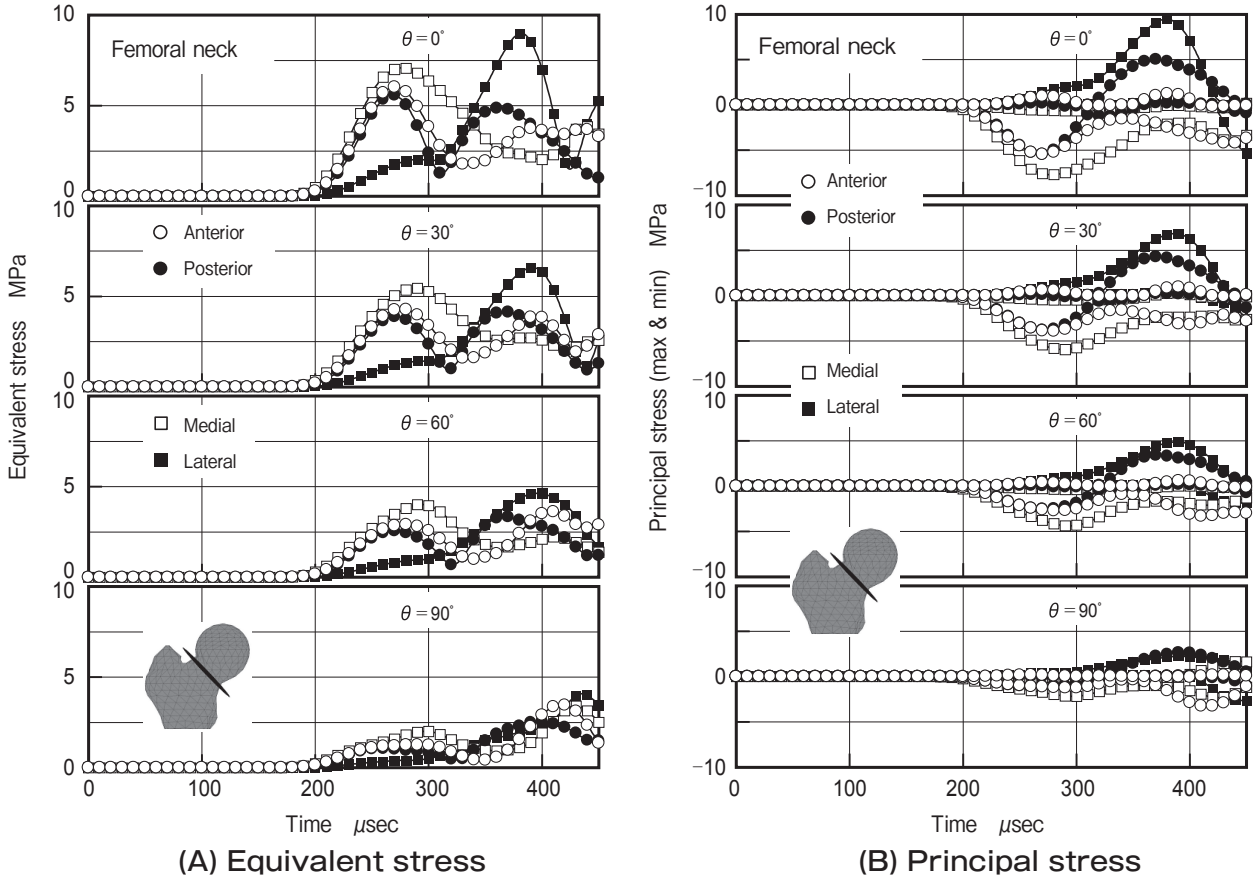

Fig. 6 Time history of stress in the cortical bone surface of the femoral neck. Changes of equivalent stress (A) and principal stress (B) with elapsed time are evaluated for 4 nodes located around the cross section of the femoral neck shown in the figure.

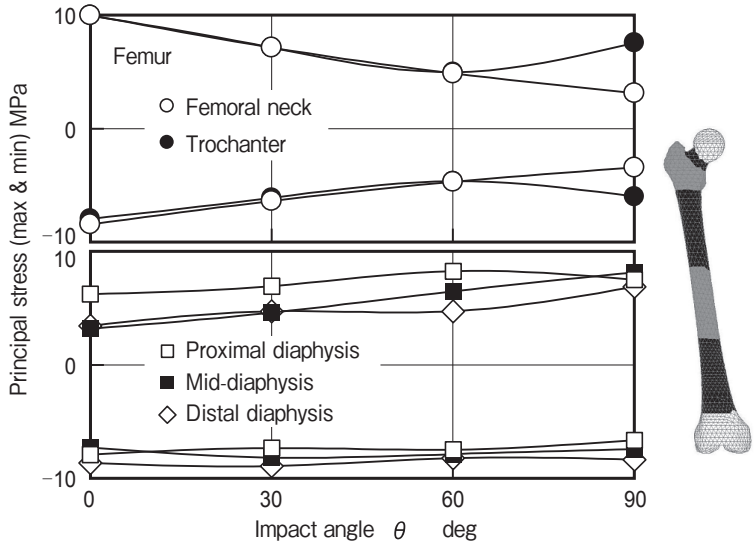

Fig. 7 Influence of impact angle on the largest absolute values of the maximum and minimum principal stress during propagation of the stress wave (t = 0–450 μsec). The largest values are obtained in the 5 regions of the femur shown in the figure.

The absolute value of the principal stress in the femoral neck became small when the impact angle increased.

We evaluated the largest absolute values of maximum and minimum principal stress during the propagation of the stress wave (t = 0–450 μsec) in the femoral neck, trochanter, proximal diaphysis, mid-diaphysis, and distal diaphysis. The relations between the largest absolute values of these 2 types of stress and the impact angles are shown in Fig. 7, where the reference region of the femur is represented in the figure. The maximum and minimum principal stress of the femoral neck and the trochanter were dependent on the impact angle, and the maximum principal stress in the case of $\theta = 0°$ was the largest for all impact angles. The influence of the impact angle on the minimum principal stress of the diaphysis was relatively small, and the minimum principal stress was not much affected by the location in the diaphysis. The maximum principal stress of the diaphysis was larger than that of the femoral neck for the large impact angle, and, especially, the maximum principal stress of the proximal diaphysis was larger than that of the neck and the trochanter in the case of $\theta = 60°$.

Discussion

There is a difference in stress distributions in the mid-diaphysis between the results for $\theta = 0°$ and $\theta = 60°$, as shown in Fig. 3. At $\theta = 0°$ the relevant stress is compressive stress, and the absolute value of the stress is large in the cortical bone. This is due to the difference of the elastic modulus; in this case the modulus of the cortical bone is larger than that of the cancellous bone. The impact direction is coincident with the bone axis in the case of $\theta = 0°$, so an almost uniaxial stress state is caused by the compressive impact. On the other hand, the impact direction is different from the bone axis in the case of $\theta = 60°$, and the impact bending is additionally applied to the diaphysis. Therefore, the stress is compression on the anterior side and tension on the posterior side, as seen in Fig. 4(B). As a result, the impact bending results in the distribution of equivalent stress at t = 300 μsec as shown in Fig. 3(B).

As for the proximal femur, the stress concentration is found around the femoral neck. The maximum principal stress indicates a large tensile value on the lateral side when the impact angle is small. It appears that the stress wave is reflected in a complicated fashion around the femoral head and the greater trochanter, and the tensile stress is due to the reflection of the stress wave. The tensile strength of the femur is generally low compared with its compressive strength [14]. As shown by the results with the small impact angle in Fig. 6(B), the absolute value of the maximum principal stress on the lateral side of the femoral neck

is larger than that of the minimum principal stress on the medial side. Bone fracture due to tensile stress may be found on the lateral side even when the fracture does not occur on the medial side. The direction of principal stress which may cause bone fracture is nearly coincident with the direction of the bone axis at the diaphysis. The direction at the femoral neck is almost parallel to the axis of the neck. These directions are roughly perpendicular to the fracture surfaces of the bone frequently observed in clinical settings.

As shown in Fig. 7, the largest tensile stress is found in the femoral neck and the trochanter when the impact is applied in the direction of the bone axis. In this case, the region of the trochanter does not include the greater trochanter, judging from the results shown in Fig. 5(A). The tensile stress is the largest at the proximal diaphysis in the case of $\theta = 60°$, indicating that this region has a higher risk of bone fracture than that of the femoral neck or the trochanter. The location of the largest tensile stress in the femur is determined by the impact angle.

The value of impulsive stress is generally proportional to the impact velocity. The bone strength of osteoporosis patients is low compared with that of healthy adults. These patients have a risk of bone fracture even when the impact is not very severe. The femoral bone has isotropic properties in the deformation, and the cancellous bone is treated as bulk tissue in the analysis. The present model should be improved considering the elastic anisotropy of the bone and the trabecular structure of the cancellous bone. The anisotropic properties of the bone have not been precisely evaluated; the creation of a finite element model of trabecular structures is very challenging.

References

1. Lotz JC, Cheal EJ and Hayes WC: Fracture Prediction for the Proximal Femur Using Finite Element Models: Part Ⅰ- Linear Analysis. J Biomech Eng (1991) 113: 353-360.
2. Lotz JC, Cheal EJ and Hayes WC: Fracture Prediction for the Proximal Femur Using Finite Element Models: Part Ⅱ- Nonlinear Analysis. J Biomech Eng (1991) 113: 361-365.
3. Keyak JH, Rossi SA, Jones KA and Skinner HB: Prediction of femoral fracture load using automated finite element modeling. J Biomech (1998) 31: 125-133.
4. Keyak JH and Rossi SA: Prediction of femoral fracture load using finite element models: an examination of stress- and strain-based failure theories. J Biomech (2000) 33: 209-214.
5. Keyak JH: Relationships between femoral fracture loads for two load configurations. J Biomech (2000) 33: 499-502.
6. Keyak JH: Improved prediction of proximal femoral fracture load using nonlinear finite element models. Med Eng Phys (2001) 23: 165-173.
7. Keyak JH, Rossi SA, Jones KA, Les CM and Skinner HB: Prediction of fracture location in the proximal femur using finite element models. Med Eng Phys (2001) 23: 657-664.
8. Bessho M, Ohnishi I, Matsuyama J, Matsumoto T, Imai K and Nakamura K: Prediction of strength and strain of the proximal femur by a CT-based finite element method. J Biomech (2007) 40: 1745-1753.
9. Bryan R, Nair PB and Taylor M: Use of a statistical model of the whole femur in a large scale, multi-model study of femoral neck fracture risk. J Biomech (2009) 42: 2171-2176.
10. Gnudi S, Ripamonti C, Gualtieri G and Malavolta N: Geometry of proximal femur in the prediction of hip fracture in osteoporotic women. Br J Radiol (1999) 72: 729-733.
11. Bergot C, Bousson V, Meunier A, Laval-Jeantet M and Laredo JD: Hip Fracture Risk and Proximal Femur Geometry from DXA Scans. Osteoporosis Int (2002) 13: 542-550.
12. Gnudi S, Malavolta N, Testi D and Viceconti M: Differences in proximal femur geometry distinguish vertebral from femoral neck fractures in osteoporotic women. Br J Radiol (2004) 77: 219-223.
13. Abé H, Hayashi K and Sato M (eds.): Data Book on Mechanical Properties of Living Cells, Tissues, and Organs. Springer-Verlag (1996): pp292-349.
14. Fung YC: Biomechanics - Mechanical Properties of Living Tissues, 2nd Ed. Springer-Verlag (1993): pp510-513.